

Radial fingering in a Hele-Shaw cell: a weakly nonlinear analysis

José A. Miranda¹ and Michael Widom²

Department of Physics

Carnegie Mellon University

Pittsburgh, PA 15213

USA

¹e-mail:01jamn@npd.ufpe.br

²e-mail:widom@andrew.cmu.edu

Abstract

The Saffman-Taylor viscous fingering instability occurs when a less viscous fluid displaces a more viscous one between narrowly spaced parallel plates in a Hele-Shaw cell. Experiments in radial flow geometry form fan-like patterns, in which fingers of different lengths compete, spread and split. Our weakly nonlinear analysis of the instability predicts these phenomena, which are beyond the scope of linear stability theory. Finger competition arises through enhanced growth of sub-harmonic perturbations, while spreading and splitting occur through the growth of harmonic modes. Nonlinear mode-coupling enhances the growth of these specific perturbations with appropriate relative phases, as we demonstrate through a symmetry analysis of the mode coupling equations. We contrast mode coupling in radial flow with rectangular flow geometry.

PACS numbers: 47.20.Ma, 47.20.Gv, 47.54.+r, 68.10.-m

Keywords: Hydrodynamic instability; Interfacial dynamics; Pattern formation; Weakly nonlinear analysis.

1 Introduction

The Saffman-Taylor problem [1] addresses motion of two viscous fluids in the narrow space between two plates, known as a Hele-Shaw cell. When a fluid of low viscosity displaces a fluid of higher viscosity, the interface between them becomes unstable and starts to deform. This problem is formally equivalent [2] to a special case of a solidification problem. Experiments and theory focus on two basic flow geometries (i) rectangular [3] and (ii) radial [4]. For both geometries, the initial developments of the interface instability tracks the predictions of linear stability theory [1]. As the unstable modes of perturbation grow, they become coupled in a weakly nonlinear stage of evolution. Finally, the system evolves to a complicated late stage, characterized by formation of fingering structures, in which nonlinear effects dominate.

This paper addresses linear and the weakly nonlinear stages of the evolution. Here we concentrate our attention on the radial flow geometry. We develop the mode coupling theory for the Saffman-Taylor problem. Our approach is a complementary study to the purely linear investigations [1] and to recent developments in the analytical [5] and numerical [6] treatments of the fully nonlinear time-evolving flow. These analytical works [5] describe

the early and late stage dynamics of the interface in the small surface tension limit, using conformal mapping techniques. Efficient numerical simulations [6] describe complex flow patterns, for both large and small surface tension, employing a boundary integral formulation of the equations of motion. On the other hand, our analytical weakly nonlinear study investigates the intermediate stage between the purely linear and the fully nonlinear ones, focusing on the onset of the nonlinear effects. Our approach applies to any value of surface tension, and gives physical insight into mechanisms of pattern solution. In the context of solidification, both numerical [7] and weakly nonlinear [8, 9] results are known.

In a separate publication [10] we develop the weakly nonlinear theory for rectangular flow geometry. Although mathematically similar to the rectangular flow problem, the radial geometry imposes two important new elements: (i) the interface is always asymmetric because of the distinction between the area inside and outside of the boundary between the fluids; (ii) the radial flow presents multiple stages of instability, with no true steady state attainable.

Experimental and theoretical investigations are plentiful for radial flow geometry Hele-Shaw cells [1]. These experiments [4, 11, 12, 13] inject the less

viscous fluid at the center of the cell, which was previously filled with the more viscous fluid. The injection is usually performed at a constant flow rate or constant pressure. Initially, the interface (bubble) is circular. As the bubble develops, the interface undulates and fingers grow. As the size of the bubble increases, the fingers spread and their tips become blunt, creating a fan-like pattern. Next, the fingers start to split at the tip. Larger fingers shield smaller ones and the pattern develops asymmetrically, causing competition among fingers of different lengths. Spreading, splitting and competition are the three basic growth mechanisms of the viscous fingering process [14].

The linear stability of a circular interface evolving in a radial geometry flow Hele-Shaw cell was studied by Bataille [13], Wilson [15], and thereafter by Paterson [4]. More recent experimental and theoretical work study the linear stage of the radial Hele-Shaw flow in a variety of situations: Sader, Chan and Hughes [16] examined the linear stability analysis for the case of a non-Newtonian displaced fluid; Carrillo et al. [17] considered radial flow in a rotating Hele-Shaw cell; Cardoso and Woods [18] investigated the linear stability analysis of an annulus of fluid, bound by two other fluids of different viscosities. Because of the complexity of the evolution, even at the level of

linear analysis, this paper reviews certain results of the linear theory for the sake of comparison with the nonlinear analysis.

The linear stability analysis applies only to early stages of the flow. Moreover, it does not explain well the essential mechanisms of spreading, splitting and competition cited above. To analyze these effects, we develop the weakly nonlinear mode coupling theory of the radial flow in a Hele-Shaw cell. We focus on the onset of the nonlinear effects and their influence on the evolution of the unstable interface. We employ an analytical approach known as a mode coupling theory. The paper is organized as follows: section II derives a differential equation describing the early nonlinear evolution of the interface modes. In section III, we interpret results obtained in section II and investigate both the linear and weakly nonlinear evolution of the system. Our chief conclusions are presented in this section. We show that second order mode coupling explains the main features of patterning formation by coupling fundamental modes to harmonics and sub-harmonics. Symmetries of the radial flow geometry dictate the form of the mode coupling equations, influencing the shapes of growing interfaces. Section IV presents our final remarks.

2 Derivation of the mode coupling differential equation

Consider two immiscible, incompressible, viscous fluids. In a Hele-Shaw cell fluids flow in a narrow gap of thickness b , between two parallel plates (see figure 1). We assume that b is smaller than any other length scale in the problem, and therefore the system is considered to be effectively two-dimensional. Denote the viscosities of the inner and outer fluids, respectively as η_1 and η_2 . The flows are assumed to be irrotational, except at the interface. Inject fluid 1 into fluid 2 at constant flow rate Q , equal to the area covered per unit time. Between the two fluids there exists a surface tension σ .

During the flow, the interface has a perturbed shape described as $\mathcal{R} = R + \zeta(\theta, t)$, where θ represents the polar angle, and $R = R(t)$ denotes the time dependent unperturbed radius

$$R(t) = \sqrt{R_0^2 + \frac{Qt}{\pi}}. \quad (1)$$

R_0 is the unperturbed radius at $t = 0$. The analytic model we seek predicts the evolution of the interface perturbation amplitude $\zeta(\theta, t)$. The early non-linear evolution of the interface obeys a second-order mode coupling equation.

The linear evolution is most readily described in terms of the complex Fourier modes

$$\zeta_n(t) = \frac{1}{2\pi} \int_0^{2\pi} \zeta(\theta, t) \exp(-in\theta) d\theta, \quad (2)$$

where $n=0, \pm 1, \pm 2, \dots$ denotes the discrete azimuthal wave number. We remain in Fourier space for our weakly nonlinear analysis. The net perturbation is represented by

$$\zeta(\theta, t) = \sum_{n=-\infty}^{+\infty} \zeta_n(t) \exp(in\theta). \quad (3)$$

Note that we include the $n = 0$ mode in our Fourier expansion (3). This is done to keep the area $\mathcal{A} = \pi R^2 = \pi R_0^2 + Qt$ of the perturbed shape independent of the perturbation ζ . Thus we require

$$\zeta_0 = -\frac{1}{2R} \sum_{n=1}^{\infty} [|\zeta_n(t)|^2 + |\zeta_{-n}(t)|^2]. \quad (4)$$

The constant area constraint is intrinsically a nonlinear concern and is not required in linear stability analysis. Since we are interested in the early nonlinear behavior of the system, our first task is to derive a differential equation for ζ_n , correct to second order.

We will occasionally refer to the “rectangular geometry limit”. By this we mean the limit $R \rightarrow \infty$ and $Q \rightarrow \infty$ such that $Q/(2\pi R) \equiv v_\infty$ and $n/R \equiv k$

remain constant, where v_∞ is the flow velocity at infinity and k denotes the wave number of the disturbance. In this limit the interface evolution reverts to the simpler evolution of the rectangular flow geometry. For example, the constant area constraint becomes simple ($\zeta_0 = 0$) in this limit.

The relevant hydrodynamic equation is Darcy's law [1, 3]

$$-\frac{12\eta_i}{b^2}\vec{v}_i - \vec{\nabla}p_i = 0, \quad (5)$$

where $\vec{v}_i = \vec{v}_i(r, \theta)$ and $p_i = p_i(r, \theta)$ are, respectively, the velocity and pressure in fluids $i = 1$ and 2 . At the interface, the pressure difference between the two fluids is given by [1]

$$(p_1 - p_2)|_{\mathcal{R}} = \sigma (\kappa_{\parallel} + \kappa_{\perp})|_{\mathcal{R}}. \quad (6)$$

The curvature in the direction perpendicular to the plates (κ_{\perp}) is nearly constant [20, 21]. Because its gradient is nearly zero, it does not significantly affect the motion in our problem.

Due to the radial geometry, we have a somewhat complicated expression for the in-plane interface curvature [15, 19]

$$\kappa_{\parallel} = \frac{\left[r^2 + 2 \left(\frac{\partial r}{\partial \theta} \right)^2 - r \frac{\partial^2 r}{\partial \theta^2} \right]}{\left[r^2 + \left(\frac{\partial r}{\partial \theta} \right)^2 \right]^{3/2}}, \quad (7)$$

where r denotes the distance from the radial flow source. The sign convention for the curvature κ_{\parallel} is such that a circular interface has positive curvature. Keeping second order terms in the perturbation amplitude ζ , we rewrite the in-plane curvature

$$\kappa_{\parallel} = \left\{ \frac{1}{R} - \frac{1}{R^2} \left(\zeta + \frac{\partial^2 \zeta}{\partial \theta^2} \right) + \frac{1}{R^3} \left[\zeta^2 + \frac{1}{2} \left(\frac{\partial \zeta}{\partial \theta} \right)^2 + 2\zeta \frac{\partial^2 \zeta}{\partial \theta^2} \right] \right\}. \quad (8)$$

For future reference, note that only one term $(1/R^2)(\partial^2 \zeta / \partial \theta^2)$ out of six terms in equation (8) survives in the rectangular geometry limit.

Taking advantage of the irrotational and incompressible flow conditions, we define the velocity potential ϕ_i in each of the fluids, where $\vec{v}_i = -\vec{\nabla} \phi_i$. The velocity potential satisfies Laplace's equation $\nabla^2 \phi_i = 0$. Combining the velocity potential with equations (6) and (7) for the pressure difference and Darcy's law (5), we write the equation of motion

$$A \left(\frac{\phi_1|_{\mathcal{R}} + \phi_2|_{\mathcal{R}}}{2} \right) - \left(\frac{\phi_1|_{\mathcal{R}} - \phi_2|_{\mathcal{R}}}{2} \right) = -\alpha \kappa_{\parallel}, \quad (9)$$

where

$$A = \frac{\eta_2 - \eta_1}{\eta_2 + \eta_1} \quad (10)$$

is the viscosity contrast and

$$\alpha = \frac{b^2 \sigma}{12(\eta_1 + \eta_2)}. \quad (11)$$

Equation (9) drops an arbitrary constant of integration related to the definition of velocity potentials. For our weakly nonlinear analysis we are interested in second order contributions in the perturbation amplitudes. Therefore, all the quantities in equation (9) are evaluated at the perturbed interface $\mathcal{R} = R + \zeta(\theta, t)$, and not at the initial unperturbed interface position R as is usually done in linearized surface deformation problems. The nonlinear terms arise because of this important distinction.

Now define Fourier expansions for the velocity potentials ϕ_i . Far from the interface the velocity field should approach the unperturbed steady flow with a circular interface of radius R . Thus for $r \rightarrow 0$ and $r \rightarrow +\infty$ the velocity potentials ϕ_i approach ϕ_i^0 , the velocity potentials for radial flow

$$\phi_i^0 = -\frac{Q}{2\pi} \log\left(\frac{r}{R}\right) + C_i. \quad (12)$$

C_i are independent of r and θ . They do not contribute to the velocity fields \vec{v}_i , so we will not discuss them further. The general velocity potentials obeying these requirements are

$$\phi_1 = \phi_1^0 + \sum_{n \neq 0} \phi_{1n}(t) \left(\frac{r}{R}\right)^{|n|} \exp(in\theta), \quad (13)$$

and

$$\phi_2 = \phi_2^0 + \sum_{n \neq 0} \phi_{2n}(t) \left(\frac{R}{r}\right)^{|n|} \exp(in\theta). \quad (14)$$

The algebraic dependence on r transforms, in the rectangular geometry limit, into exponential dependence. In order to calculate the mode coupling differential equation for the system, we substitute expansions (12), (13) and (14) into the equation of motion (9), keep second order terms in the perturbation amplitudes, and Fourier transform them.

We need additional relations expressing the velocity potentials in terms of the perturbation amplitudes. To find these, consider the kinematic boundary condition which states that the normal components of each fluid's velocity at the interface equals the velocity of the interface itself [22]. In polar coordinates (r, θ) the kinematic boundary condition is written as

$$\frac{\partial \mathcal{R}}{\partial t} = \left(\frac{1}{r^2} \frac{\partial \mathcal{R}}{\partial \theta} \frac{\partial \phi_i}{\partial \theta} \right)_{r=\mathcal{R}} - \left(\frac{\partial \phi_i}{\partial r} \right)_{r=\mathcal{R}}. \quad (15)$$

Expand the boundary condition equation (15) to second order in ζ and then Fourier transform. The constraint that area \mathcal{A} be independent of the perturbation ζ (equation (4)) enforces the equality of the $n = 0$ Fourier mode on each side of equation (15). Nontrivial identities are obtained for $n \neq 0$.

Solving for $\phi_{in}(t)$ consistently to second order in ζ yields

$$\begin{aligned}\phi_{1n}(t) &= -\frac{R}{|n|}\dot{\zeta}_n - \frac{Q}{2\pi R|n|}\zeta_n \\ &+ \sum_{n' \neq 0} \left(\text{sgn}(nn') - \frac{1}{|n|} \right) \dot{\zeta}_{n'} \zeta_{n-n'} + \frac{Q}{2\pi R^2} \sum_{n' \neq 0} \text{sgn}(nn') \zeta_{n'} \zeta_{n-n'},\end{aligned}\tag{16}$$

and

$$\begin{aligned}\phi_{2n}(t) &= \frac{R}{|n|}\dot{\zeta}_n + \frac{Q}{2\pi R|n|}\zeta_n \\ &+ \sum_{n' \neq 0} \left(\text{sgn}(nn') + \frac{1}{|n|} \right) \dot{\zeta}_{n'} \zeta_{n-n'} + \frac{Q}{2\pi R^2} \sum_{n' \neq 0} \text{sgn}(nn') \zeta_{n'} \zeta_{n-n'}.\end{aligned}\tag{17}$$

The overdot denotes total time derivative. The sign function $\text{sgn}(nn') = 1$ if $(nn') > 0$ and $\text{sgn}(nn') = -1$ if $(nn') < 0$. We can use relations (16) and (17) to replace the velocity potentials ϕ_i in Darcy's law (9) with the perturbation ζ and its time derivative $\dot{\zeta}$. Keeping only quadratic terms in the perturbation amplitude, and equating Fourier modes n on each side of Darcy's law, leads to the differential equation for perturbation amplitudes ζ_n . For $n \neq 0$,

$$\dot{\zeta}_n = \lambda(n)\zeta_n + \sum_{n' \neq 0} \left[F(n, n') \zeta_{n'} \zeta_{n-n'} + G(n, n') \dot{\zeta}_{n'} \zeta_{n-n'} \right], \tag{18}$$

where

$$\lambda(n) = \left[\frac{Q}{2\pi R^2} (A|n| - 1) - \frac{\alpha}{R^3} |n|(n^2 - 1) \right], \quad (19)$$

and

$$F(n, n') = \frac{|n|}{R} \left\{ \frac{QA}{2\pi R^2} \left[\frac{1}{2} - \text{sgn}(nn') \right] - \frac{\alpha}{R^3} \left[1 - \frac{n'}{2}(3n' + n) \right] \right\}, \quad (20)$$

$$G(n, n') = \frac{1}{R} \{ A|n|[1 - \text{sgn}(nn')] - 1 \}. \quad (21)$$

Equation (18) is the mode coupling equation of the Saffman-Taylor problem in a radial flow geometry Hele-Shaw cell. It gives us the time evolution of the perturbation amplitudes ζ_n accurate to second order. The first term on the right-hand side of equation (18) reproduces the linear stability analysis [4, 13, 15], where $\lambda(n)$ denotes the linear growth rate. The remaining terms represent second-order mode coupling in a radial flow geometry. They arise as a direct consequence of our weakly nonlinear analysis, which considers the presence of a full spectrum of modes.

It is interesting to compare the radial geometry mode coupling equation with the rectangular geometry result [10]. Several terms simplify. In particular,

$$\lambda(n) \rightarrow |k| \left[Av_\infty - \alpha k^2 \right] \quad (22)$$

$$F(n, n') \rightarrow 0 \tag{23}$$

$$G(n, n') \rightarrow A|k| [1 - \text{sgn}(kk')]. \tag{24}$$

When k and k' are parallel there is no second order mode coupling in the rectangular geometry limit. Note that, in contrast to the radial geometry expression (19), the rectangular geometry linear growth rate (22) is not time dependent. The approach of each term to its limit is $\mathcal{O}(1/R)$. In the following section we investigate the radial geometry equation (18) in more detail.

3 Discussion

3.1 Linear evolution

Considering the complexity of the flow, we begin by analyzing certain aspects of the linear theory. This analysis is needed for our subsequent weakly nonlinear investigation (section 3.2). First consider the purely linear contribution, which appears as the first term on the right hand side of equation (18). Since R varies with time, the linear growth rate $\lambda(n)$ is time dependent as well. This implies that the actual relaxation or growth of mode n is not

proportional to the factor $\exp[\lambda(n)t]$, but rather

$$\zeta_n(t) = \zeta_n(0) \exp \left[\int_0^t \lambda(n) dt' \right]. \quad (25)$$

If $\int_0^t \lambda(n) dt' > 0$ the disturbance grows, indicating instability. Inspecting equation (19) for $\lambda(n)$ we notice opposing effects of the viscosity difference between the fluids (destabilizing) and of the surface tension at the interface (stabilizing). Two other relevant facts can be extracted from the linear growth rate: (i) the existence of a series of critical radii at which the interface becomes unstable for a given mode n (defined by setting $\lambda(n) = 0$),

$$R_c(n) = \frac{2\pi\alpha}{Q} \frac{|n|(n^2 - 1)}{(A|n| - 1)}; \quad (26)$$

(ii) the presence of a fastest growing mode n^* , given by the closest integer to the maximum of equation (19) with respect to n (defined by setting $d\lambda(n)/dn = 0$),

$$n_{max}(R) = \pm \sqrt{\frac{1}{3} \left(\frac{QRA}{2\pi\alpha} + 1 \right)}. \quad (27)$$

Note that n^* varies with time. In view of equation (25) n^* is not simply related to the number of fingers present, even in the early stages of pattern formation. Furthermore, in the nonlinear regime the subsequent tip-splitting

process and mode competition result in a final number of fingers which can differ from the number present in the linear regime.

Inspired by a model developed by Cardoso and Woods [18] (their “model B”), we describe the behavior of the system assuming the presence of a constant low level of noise during the whole evolution of the interface. The sources of noise may come, for instance, from inhomogeneities on the surface of the Hele-Shaw cell, irregularities in the gap thickness b , or even from thermal or pressure fluctuations [23]. The predictions of this model are in qualitative agreement with experimental observations within the linear regime [18]. We perform a detailed investigation of this model in the linear regime and extend its range of applicability to the weakly nonlinear stage of evolution.

Suppose that we begin with an initially circular interface that is steadily expanding. During the interface expansion each mode n is perturbed with a constant (in time) random complex amplitude $\zeta_n(0)$. This noise amplitude contains an n dependent random phase but its magnitude $|\zeta_n(0)|$ is independent of n by assumption. As the interface continues to expand, it progressively reaches critical radii $R_c(n)$ for $n = 2, 3, \dots$. Once a particular $R_c(n)$ is reached, the perturbation amplitude ζ_n starts to vary with time.

Within this model, the first order (linear) solution of equation (18) can be written as

$$\zeta_n^{lin}(t) = \begin{cases} \zeta_n(0) & \text{if } R < R_c(n) \\ \zeta_n(0) \left\{ \left(\frac{R}{R_c(n)} \right)^{A|n|-1} \exp \left[(A|n| - 1) \left(\frac{R_c(n)}{R} - 1 \right) \right] \right\} & \text{if } R \geq R_c(n). \end{cases} \quad (28)$$

To further analyze the behavior of the linear solution equation (28) and see the overall effect of the above mentioned properties, we plot the time evolution of the interface. It is convenient to rewrite the net perturbation (3) in terms of sine and cosine modes

$$\zeta(\theta, t) = \zeta_0 + \sum_{n=1}^{\infty} [a_n(t) \cos(n\theta) + b_n(t) \sin(n\theta)], \quad (29)$$

where $a_n = \zeta_n + \zeta_{-n}$ and $b_n = i(\zeta_n - \zeta_{-n})$ are real-valued. Throughout this work we use the experimental parameters given in Paterson's classical experiment [4]. Paterson observed the rapid growth of fingers, as air ($\eta_1 \approx 0$) was blown at a relatively high injection rate, $Q = 9.3 \text{ cm}^2/\text{s}$, into glycerine ($\eta_2 \approx 5.21 \text{ g}/(\text{cm s})$) in a radial source flow Hele-Shaw cell. The thickness of the cell $b = 0.15 \text{ cm}$ and the surface tension $\sigma = 63 \text{ dyne/cm}$. We take into account modes n ranging from $n = 2$ up to 20. We evolve from initial radius $R_0 = 0.05 \text{ cm}$. The noise amplitude $|\zeta_n(0)| = R_0/500$. Figure 2, depicts the

evolution of the interface, for a random choice of phases, up to time $t = 30$ s.

Linear evolution proceeds through a cascade of modes, with increasing participation of higher modes n as time progresses. The number of fingers is typically given by the mode n which has grown to largest amplitude. Variability of finger lengths depends primarily on modes of smaller n . Modes of larger n can cause the tips of the fingers to split. For the early evolution of the interface, patterns like those shown in figure 2 resemble well the experimental patterns found in the literature [4, 11, 12, 13].

In contrast to the experiments, some important features are not present in figure 2, revealing failure of the purely linear approach. Spreading of the fingers, which is observed in the experiments, is not clearly shown in figure 2. Experimentally, the tips of fingers tend to split. To observe finger-splitting using the linear theory, we would have to go to unrealistically long times. Finger competition, also, is not as pronounced in the linear theory as in experiment. These last few remarks indicate that, despite being an adequate approximation for early times, a purely linear theory does not describe all the basic physical mechanisms (spreading, splitting and competition) involved in

the pattern formation. The linear regime is valid only for a limited initial period beyond which nonlinear effects take over.

3.2 Weakly nonlinear evolution

The nonlinear effects considered here come from the contributions of the second term on the right hand side of equation (18). Let us begin by briefly describing the various pieces appearing in this second term. The function $F(n, n')$, which multiplies the term $\zeta_{n'}\zeta_{n-n'}$, presents two parts (see equation (20)) having distinct origins: the first one comes from the unperturbed radial flow (equation (12)) evaluated at the perturbed interface \mathcal{R} , while the second one arises from the second order terms in ζ present in the curvature (see equation (8)). Neither term survives in the rectangular geometry limit. On the other hand, the function $G(n, n')$ (see equation (21)) multiplies the term $\dot{\zeta}_{n'}\dot{\zeta}_{n-n'}$, which couples the perturbed flow $\dot{\zeta}$ with the interface shape perturbation ζ . Only the $\mathcal{O}(1/R)$ part of $G(n, n')$ depends on the curvature of the unperturbed interface.

To visualize the implications of mode coupling, we solve equation (18) to second order accuracy. If we substitute the linear solution given in equa-

tion (28) into the second-order terms on the right hand side of equation (18), we obtain the differential equation

$$\dot{\zeta}_n = \lambda(n)\zeta_n + W(n, t), \quad (30)$$

where

$$W(n, t) = \sum_{n' \neq 0} \left[F(n, n') \zeta_{n'}^{lin} \zeta_{n-n'}^{lin} + G(n, n') \dot{\zeta}_{n'}^{lin} \zeta_{n-n'}^{lin} \right] \quad (31)$$

acts as a driving force in the linearized equation of motion (30). Despite the complicated form of the functions $\lambda(n)$ and $W(n, t)$, equation (30) is a standard first order linear differential equation [24] with the solution

$$\zeta_n(t) = \begin{cases} \zeta_n(0) & \text{if } R < R_c(n) \\ \zeta_n^{lin}(t) \left\{ 1 + \int_{t_c(n)}^t \left[\frac{W(n, t')}{\zeta_n^{lin}(t')} \right] dt' \right\} & \text{if } R \geq R_c(n). \end{cases} \quad (32)$$

Here $t_c(n)$ is the time required for the unperturbed growth to reach radius $R_c(n)$ and can be easily calculated from equation (1). This solution describes the weakly nonlinear evolution, where the dominant modes just become coupled by nonlinear effects.

We use the second order solution (32) to investigate the nonlinear coupling among various modes n . Once again, we use the sine and cosine mode representation for the net perturbation $\zeta(\theta, t)$. In figure 3, we plot the interface for a certain time ($t = 30$ s), considering the same random choice

of initial phases as was employed in figure 2, and coupling all modes with $2 \leq n \leq 20$. The solid curve represents the interface shape obtained from the mode coupling solution (32), and the dashed line represents the interface in the linear approximation (taken from figure 2). The two interfaces are plotted together to facilitate comparison between the linear and nonlinear approaches. As we can see, the nonlinear evolution leads to wider fingers and their tips become more blunt. These fingers spread and some of them start to bifurcate, by splitting at the tip. The onset of finger competition is also observed, with some fingers slightly enhanced and others diminished.

Even though the differences between the two evolutions are not dramatic, we see that the nonlinear approach developed here leads to a more realistic description of the radial fingering patterns. The effects of finger spreading, finger tip-splitting and finger competition are all present. The fact that the second order pattern is quantitatively close to the linear pattern suggests that the nonlinearities are fairly accurately described up to $t = 30$ s by second order mode coupling theory, because the contributions of third and higher order terms should be smaller yet.

One interesting point to be discussed is the evolution of a particular mode

and its interaction with its sub-harmonics and harmonics (figure 4). Here we concentrate our attention on a small number of modes. This situation is obviously idealized compared with interaction of all modes illustrated in figure 3, but it gives us good indications about the role of mode coupling during interface evolution.

For convenience we write the explicit equations of motion in the sine and cosine representation of the interface. The even and odd functions $a_n \cos(n\theta)$ and $b_n \sin(n\theta)$ form representations (respectively, the identity A_1 , and the reflection antisymmetric representation A_2) of the rotation and reflection symmetry group C_{nv} [25]. The signs, and relative magnitudes, of a_n and b_n determine the phase of mode n . In real space, they determine the location of the n fingers on the growing perimeter. In addition to these one-dimensional representations, C_{nv} has a set of two dimensional irreducible representations $\{E_m\}$ formed by the cosine and sine functions of mode $m = 1, 2, \dots$, up to the largest integer less than $n/2$. Modes $m' > n/2$ transform identically to modes $m = n - m' < n/2$. When n is even, $m = m' = n/2$ is an integer, and the representation $E_{n/2}$ decomposes into a pair of reflection symmetric and antisymmetric representations B_1 and B_2 .

The transformation properties of modes under rotations and reflections guarantee invariance of their equations of motion, but constrain the forms of those equations. Symmetry dictates which products of modes appear in each equation of motion. The numerical values of the coefficients multiplying these products, however, can only be obtained from a full derivation of the equation of motion such as we presented in section 2. Symmetry issues have been addressed in studies of shape selection for Saffman-Taylor fingers in rectangular channels [26, 27] and crystal growth processes [28, 29, 30].

First, we consider the influence of a fundamental mode on the growth of its harmonic. We take n as the fundamental and $2n$ as the harmonic. Without loss of generality we may take the phase of the fundamental so that $a_n > 0$ and $b_n = 0$. We also replace \dot{a}_n with $\lambda(n)a_n$ in terms already of second order. The equations of motion become

$$\dot{a}_{2n} = \lambda(2n)a_{2n} + \frac{1}{2} [F(2n, n) + \lambda(n)G(2n, n)] a_n^2 \quad (33)$$

$$\dot{b}_{2n} = \lambda(2n)b_{2n}. \quad (34)$$

To see how symmetries constrain the form of these equations, we employ the group C_{2nv} . The fundamental a_n transforms as representation B_1 , while

the harmonic a_{2n} transforms as the identity representation A_1 . The product of B_1 with itself equals the identity representation, so a term of the form a_n^2 appears in equation (33). In contrast, b_{2n} transforms as the reflection antisymmetric representation A_2 , which cannot be formed from a product of the representation B_1 with any other representation present. Consequently a_n cannot influence the growth of b_{2n} at second order.

Note that $(1/2)[F(2n, n) + \lambda(n)G(2n, n)] < 0$. At second order, the result is a driving term of order a_n^2 forcing growth of $a_{2n} < 0$. With this particular phase of the harmonic forced by the dynamics, the n fingers of the fundamental mode n tend, first, to spread and blunt, and later, to split. See figure 4 for an illustration. The solid line exhibits the broadened and split fingers predicted by the nonlinear mode coupling, while the dashed line shows the linear theory for comparison. Had growth of $a_{2n} > 0$ been favored, fingers would have sharpened instead of blunting. Mode b_{2n} , whose growth is uninfluenced by a_n , skews the fingers of mode n . In the presence of $a_{2n} < 0$, the role of b_{2n} is to favor one of the two split fingers over the other. The driving term in equation of motion (33) spontaneously generates the harmonic mode, even in the absence of random noise. This effect is clearly shown in

the numerical solution of a solidification model [7].

In the rectangular geometry limit the driving term vanishes. Finger splitting thus depends on the curvature of the unperturbed interface. Finger spreading and splitting is a unique prediction of the second order mode coupling in the radial geometry.

Next, consider the influence of a fundamental mode n , assuming n is even, on the growth of its sub-harmonic mode $n/2$. Again, without loss of generality, we may choose the phase for the fundamental to set $a_n > 0$ and $b_n = 0$. The equations of motion become

$$\dot{a}_{n/2} = \left\{ \lambda(n/2) + \frac{1}{2} \left[F \left(-\frac{n}{2}, \frac{n}{2} \right) + \lambda(n/2) G \left(\frac{n}{2}, -\frac{n}{2} \right) \right] a_n \right\} a_{n/2} \quad (35)$$

$$\dot{b}_{n/2} = \left\{ \lambda(n/2) - \frac{1}{2} \left[F \left(-\frac{n}{2}, \frac{n}{2} \right) + \lambda(n/2) G \left(\frac{n}{2}, -\frac{n}{2} \right) \right] a_n \right\} b_{n/2}. \quad (36)$$

As in our analysis of the growth of the harmonic (equations (33) and (34)) the multiplication of representations dictates the form of the equations of motion. We employ the symmetry group C_{nv} . Mode n forms the identity representation A_1 . Note that $a_{n/2}$ and $b_{n/2}$ transform as representations B_1 and B_2 . Had we taken n odd, there would be no sub-harmonic $n/2$. However, the cosine and sine modes m transform as two-dimensional representations

E_m for $m < n/2$ and $E_{n-m'}$ for $m' > n/2$. Consider a pair of modes m and $m' = n - m$. The product of the fundamental mode n with mode m' transforms as mode m . Consequently mode n and m' together would influence the growth of mode m . The special case under consideration has n even, and $m = m' = n/2$.

Note that $(1/2) [F(-n/2, n/2) + \lambda(n/2)G(n/2, -n/2)] > 0$. The fundamental thus enhances the growth of its even sub-harmonic while inhibiting growth of its odd sub-harmonic. The result is to favor perturbations $a_{n/2}$ which break the n -fold rotational symmetry of the fundamental by alternately increasing and decreasing the length of each of the n fingers. This effect describes finger competition. In contrast, mode $b_{n/2}$ skews the fingers while varying the depths of the valleys between fingers. Whereas the equations of motion for the harmonic (equations (33) and (34)) contain a driving term, the equations of motion for the sub-harmonic (equations (35) and (36)) show that rotational symmetry breaking sub-harmonics must be introduced through noise or initial conditions. They cannot grow spontaneously. The sign of $a_{n/2}$ is not determined by the equation of motion. Positive and negative values of $a_{n/2}$ determine which fingers grow at the expense of the others.

Finger competition with $a_{n/2} > 0$ is evident in figure 4. Reflection-symmetry breaking perturbations $b_{n/2}$ are suppressed consistent with known properties of selected steady state patterns [26, 27].

Finally, consider the influence of a mode on itself. Consider $a_n > 0$ and $b_n = 0$. There is no $\mathcal{O}(a_n^2)$ term in the equation of motion, consistent with the demands of $C_{\infty v}$ invariance of the radial geometry equations of motion. However, our discussion above shows that a fundamental mode n spontaneously generates its own harmonic $a_{2n} < 0$ of order a_n^2 . This harmonic couples back into the equation of motion for a_n (replace $n/2 \rightarrow n$ in equation (35)), resulting in an $\mathcal{O}(a_n^3)$ diminution over the linear growth of a_n . In real space, a growing finger broadens as it pushes into the more viscous fluid. The broadened finger becomes increasingly resistant to further growth. The third order coupling of a mode with itself was studied in related solidification models [8, 9].

In order to reinforce the conclusions of the previous paragraphs, compare the time evolution of the fundamental, harmonic and sub-harmonic perturbation amplitudes following the linear (28) and nonlinear (32) solutions. In figure 5 we present the time evolution of the perturbation amplitudes a_n for

the modes $n=4, 8$ and 16 as given by the simple linear superposition of these modes (dashed curves) and by our weakly nonlinear mode coupling theory (solid curves). We observe that the weakly nonlinear coupling dictates the enhanced growth of both sub-harmonic (a_4) and first harmonic (a_{16}) modes while diminishing the growth of the fundamental (a_8). The sign of the harmonic (a_{16}) is dictated as well, going strongly negative although its initial value was positive. Therefore, the nonlinear effects naturally enhance finger competition and tendency to finger tip-splitting.

4 Concluding remarks

In this paper, we studied the onset of nonlinear effects in the radial viscous fingering in a Hele-Shaw cell. While reasonably accurate for the initial stages of the flow, linear stability theories do not explain well the origin of the essential mechanisms of finger spreading, finger tip-splitting and finger competition. We derived a second order mode coupling differential equation for the perturbation amplitudes. By considering the interaction of a small number of modes, we revealed the role of sub-harmonic and harmonic per-

turbations at the onset of pattern formation. Symmetries of the radial flow geometry constrain the form of the mode coupling equations. Mode coupling provides a mechanism for finger spreading, splitting and competition creating patterns consistent with those observed in experiments. Reflection-symmetric fingers are favored. Our analytical mode coupling approach links the simple initial linear behavior with the strongly nonlinear advanced stages of evolution.

We compared the radial flow geometry with the simpler case of flow in rectangular channels [10]. The rectangular geometry represents a special case of the radial flow, in which effects of curvature of the unperturbed interface vanish. Finger splitting, in the radial flow geometry, is driven by curvature of the unperturbed interface. Tendency towards finger splitting may be controlled by adjusting this interfacial curvature. Presumably similar control is possible by performing the flow in curved two-dimensional spaces. Such effectively two-dimensional curved spaces may be found between curved surfaces embedded in three dimensions, separated from each other by a small distance b . Positive spatial curvature (e.g., flow between concentric spheres) should inhibit finger splitting while negative curvature (e.g., flow between

saddle shape surfaces) should enhance it.

Finally, the weakly nonlinear approach we developed in this paper and in reference [10] will be useful to investigate the onset of nonlinear effects in hydrodynamic stability problems involving ferrofluids [22, 31] and lipid domains [32].

Acknowledgments

This work was supported in part by the National Science Foundation grant No. DMR-9221596. J.A.M. (CNPq reference number 200204/93-9) would like to thank CNPq (Brazilian Research Council) for financial support. We acknowledge useful discussions with Steve Garoff, David Jasnow and Robert F. Sekerka.

References

- [1] For review articles on this subject, see for instance, D. Bensimon, L. P. Kadanoff, S. Liang, B. I. Shraiman and C. Tang, *Rev. Mod. Phys.* **58**, 977 (1986); S. Tanveer, in *Asymptotics beyond all orders*, 1991, NATO ASI series B, vol. **284**, p. 131, edited by H. Segur, S. Tanveer and H. Levine (Plenum, New York, 1991); K. V. McCloud and J. V. Maher, *Phys. Rep.* **260**, 139 (1995). See also reference [14].
- [2] E. Ben-Jacob, *Nature* **343**, 523 (1990).
- [3] P. G. Saffman and G. I. Taylor, *Proc. R. Soc. London Ser. A* **245**, 312 (1958).
- [4] L. Paterson, *J. Fluid Mech.* **113**, 513 (1981).
- [5] M. Siegel, S. Tanveer and W.-S. Dai, *J. Fluid Mech.* **323**, 201 (1996) and references therein; S. Tanveer, *Phil. Trans. R. Soc. Lond. A* **343**, 155 (1993).
- [6] T. Y. Hou, J. S. Lowengrub and M. J. Shelley, *J. Comp. Phys.* **114**, 312 (1994); W.-S. Dai and M. J. Shelley, *Phys. Fluids A* **5**, 2131 (1993).

- [7] L. N. Brush and R. F. Sekerka, *J. Crystal Growth* **96**, 419 (1989).
- [8] L. N. Brush, R. F. Sekerka and G. B. McFadden, *J. Crystal Growth* **100**, 89 (1990).
- [9] P. P. Debroy and R. F. Sekerka, *Phys. Rev. E* **53**, 6244 (1996).
- [10] J. A. Miranda and M. Widom (preprint, 1997).
- [11] J.-D. Chen, *J. Fluid Mech.* **201**, 223 (1989); J. -D. Chen, *Exp. Fluids* **5**, 363 (1987).
- [12] H. Thomé, M. Rabaud, V. Hakim and Y. Couder, *Phys. Fluids* **A1**, 224 (1989).
- [13] J. Bataille, *Revue Inst. Pétrole* **23**, 1349 (1968).
- [14] G. Homsy, *Ann. Rev. Fluid Mech.* **19**, 271 (1987).
- [15] S. D. R. Wilson, *J. Colloid Interface Sci.* **51**, 532 (1975).
- [16] J. E. Sader, D. Y. C. Chan, and B. D. Hughes, *Phys. Rev. E* **49**, 420 (1994).

- [17] Ll. Carrillo, F. X. Magdaleno, J. Casademunt and J. Ortín, Phys. Rev. E **54**, 6260 (1996).
- [18] S. S. S. Cardoso and A. W. Woods, J. Fluid Mech. **289**, 351 (1995).
- [19] B. A. Dubrovin, A. T. Fomenko, and S. P. Novikov, *Modern Geometry- Methods and Applications, Part 1* (Springer-Verlag, New York, 1984).
- [20] J. W. McLean and P. G. Saffman, J. Fluid Mech. **102**, 455 (1981); P. G. Saffman, in *Macroscopic Properties of Disordered Media*, 1982, Lecture Notes in Physics, vol. **154**, p. 208, edited by R. Burrige, S. Childress and G. Papanicolaou (Springer-Verlag, New York, 1982).
- [21] For a discussion on the influence of wall wetting effects on the curvature in the direction perpendicular to the plates, see C. -W. Park and G. M. Homsy, J. Fluid Mech. **139**, 291 (1984); D. A. Reinelt, J. Fluid Mech. **183**, 219 (1987).
- [22] R. E. Rosensweig, *Ferrohydrodynamics* (Cambridge University Press, Cambridge, 1985).
- [23] M. J. P. Gingras and Z. Rácz, Phys. Rev. A **40**, 5960 (1989).

- [24] I. S. Gradshteyn and I. M. Ryzhik, *Table of Integrals, Series, and Products* (Academic Press, New York, 1994).
- [25] L. D. Landau and E. M. Lifshitz, *Quantum Mechanics: Non-relativistic Theory* (Pergamon Press, New York, 1977).
- [26] S. Tanveer, Phys. Fluids **30**, 1589 (1987).
- [27] R. Combescot and T. Dombre, Phys. Rev. A **38**, 2573 (1988).
- [28] E. Brener, H. Müller-Krumbhaar, Y. Saito and D. Temkin, Phys. Rev. E **47**, 1151 (1993); T. Ihle and H. Müller-Krumbhaar, Phys. Rev. E **49**, 2972 (1994).
- [29] R. Kupferman, D. A. Kessler and E. Ben-Jacob, Physica A **213**, 451 (1995).
- [30] M. B. Amar and E. Brener, Physica D **98**, 128 (1996).
- [31] D. P. Jackson, R. E. Goldstein and A. O. Cebers, Phys. Rev. E **50**, 298 (1994) and references therein.
- [32] H. A. Stone and H. M. McConnell, Proc. R. Soc. London Ser. A **448**, 97 (1995) and references therein.

Figure Captions

Figure 1: Schematic configuration of the radial source flow. The viscosities of inner and outer fluids are η_1 and η_2 , respectively. Fluid 1 is injected into the Hele-Shaw cell, previously filled with fluid 2, with constant injection rate Q . The dashed line represents the unperturbed circular interface R and the solid undulated curve depicts the perturbed interface $\mathcal{R} = R + \zeta(\theta, t)$, where θ is the polar angle. The surface tension between the two fluids is given by σ and b denotes the thickness of the Hele-Shaw cell.

Figure 2: Time evolution of the interface between the fluids, as given by the linear theory, including modes $2 \leq n \leq 20$. The initial perturbation amplitudes $|\zeta_n(0)| = R_0/500$ and $R_0 = 0.05$ cm. The experimental parameters are given in the text and $t=10, 20$ and 30 s.

Figure 3: Snapshot of the interfacial patterns for $t=30$ s in the cases of linear (dashed curve) and nonlinear (solid curve) evolutions. All physical parameters and initial conditions are the same as those used in figure 2.

Figure 4: Snapshot of the interface between the two fluids ($t=30$ s), for the case of three interacting cosine modes (a fundamental $n = 8$, its sub-harmonic $n/2 = 4$ and its harmonic $2n = 16$). Initial conditions are $a_n(0)=3.5 \times 10^{-4}$ cm and $R_0 = 0.3$ cm. Other parameters are as in figures 2 and 3. The dashed (solid) curve obeys the linear (nonlinear) theory. The nonlinear contributions coming from the harmonic results in wider fingers, which tend to bifurcate. Finger competition is favored by the influence of the sub-harmonic mode.

Figure 5: Time evolution of the cosine perturbation amplitudes a_n ($n=4, 8$ and 16) for linear (dashed curves) and nonlinear (solid curves) cases. The initial conditions and physical parameters are the same as those used in figure 4.

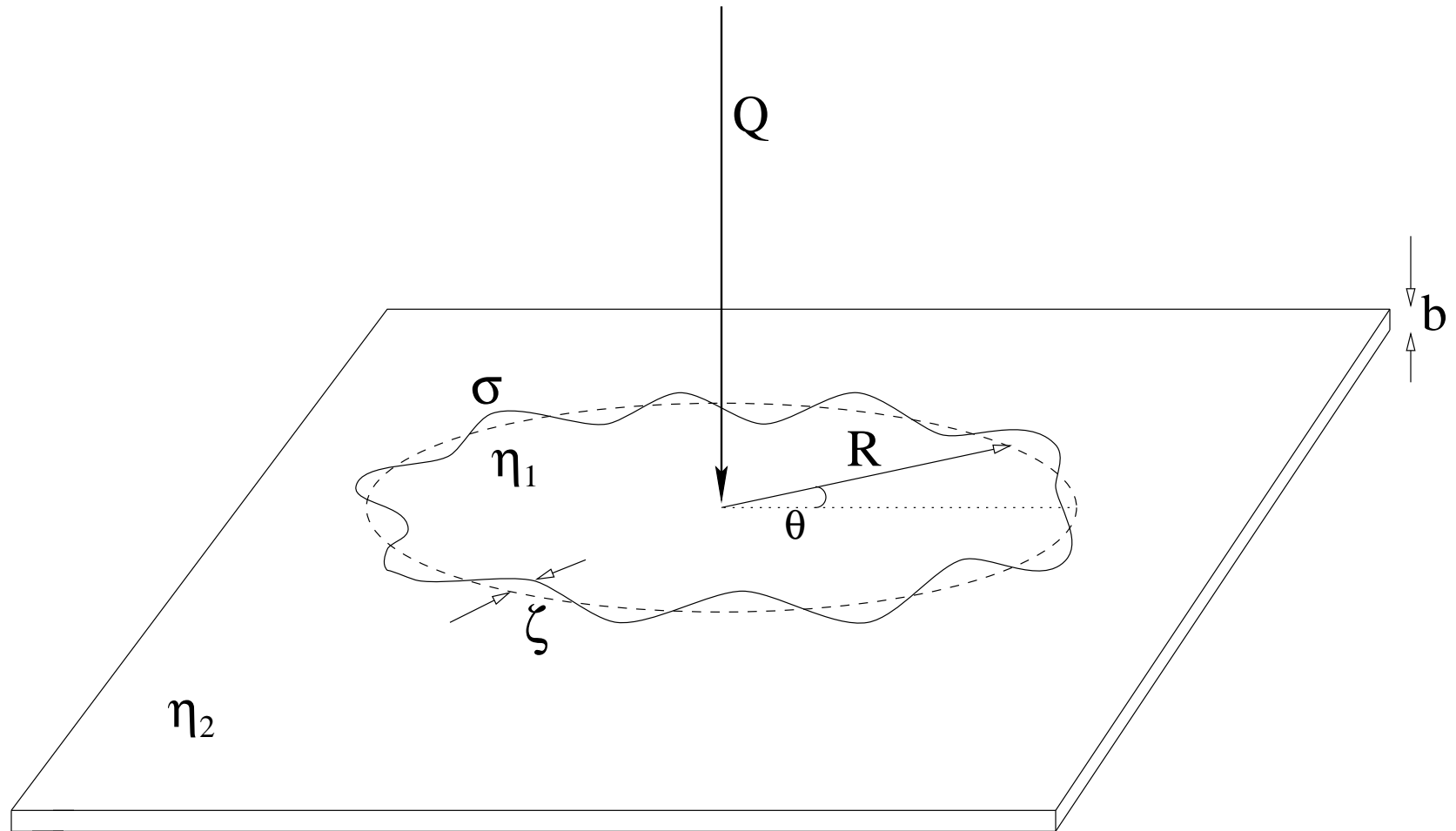


Figure 1

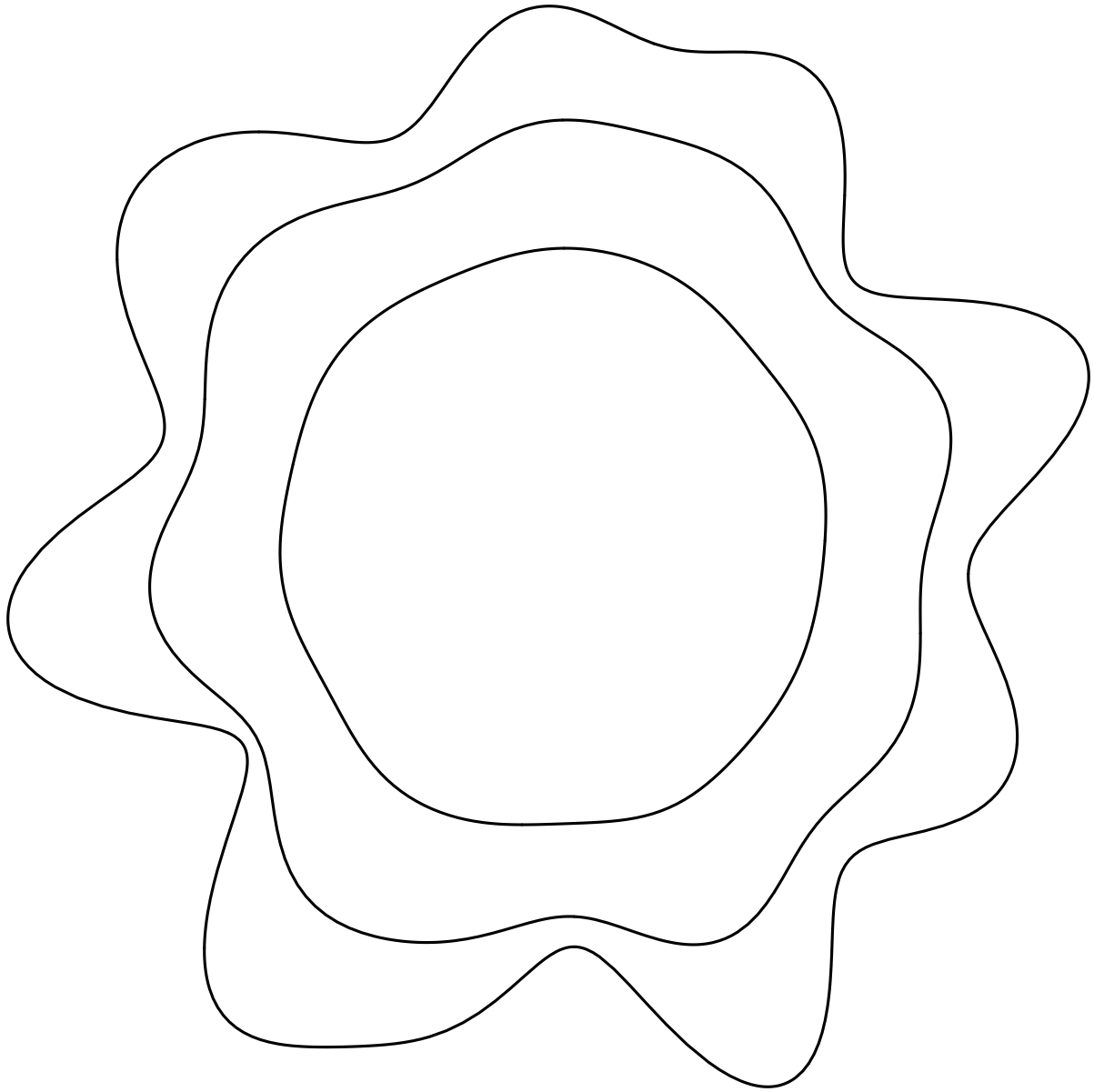


FIGURE 2

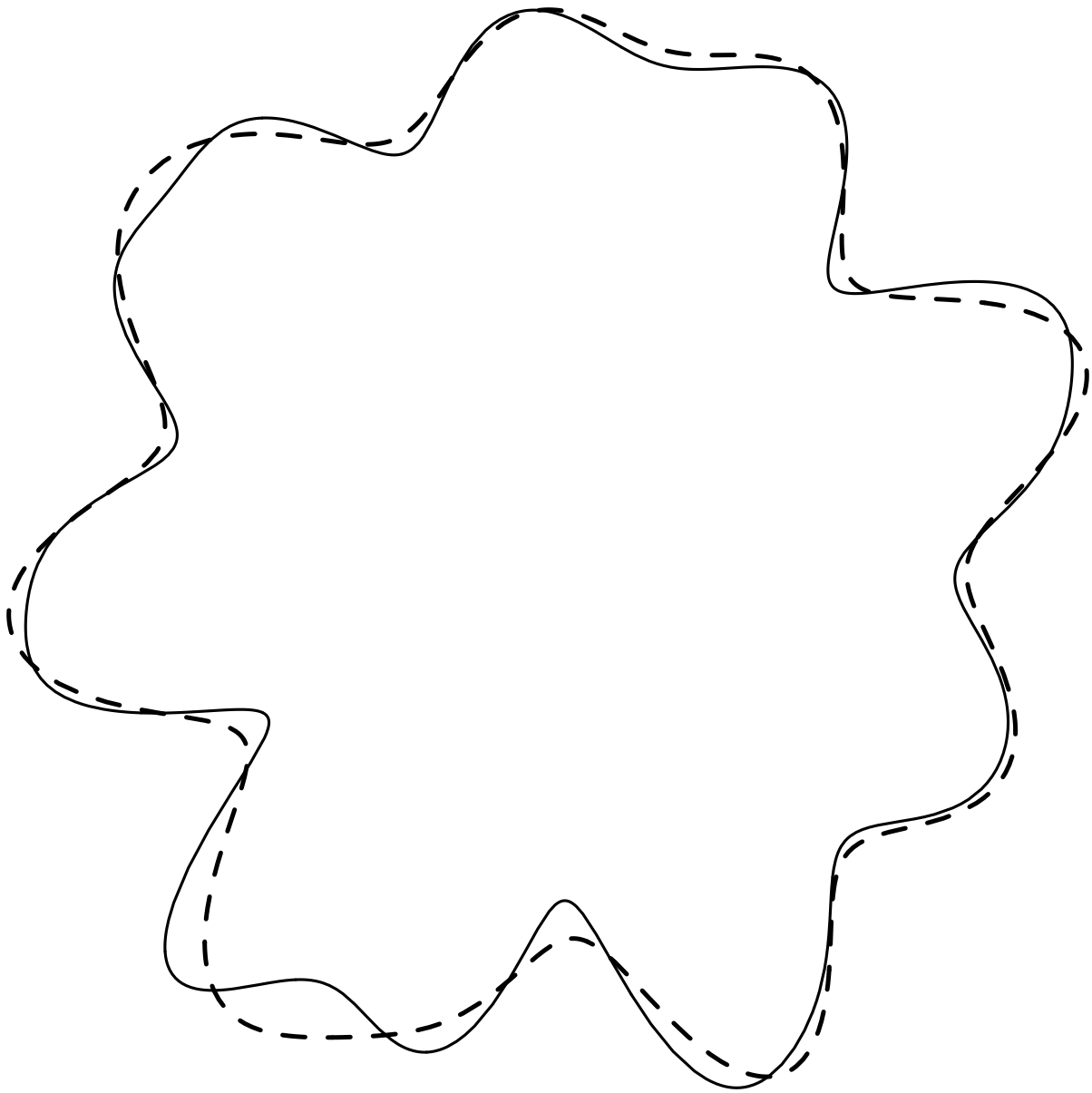


FIGURE 3

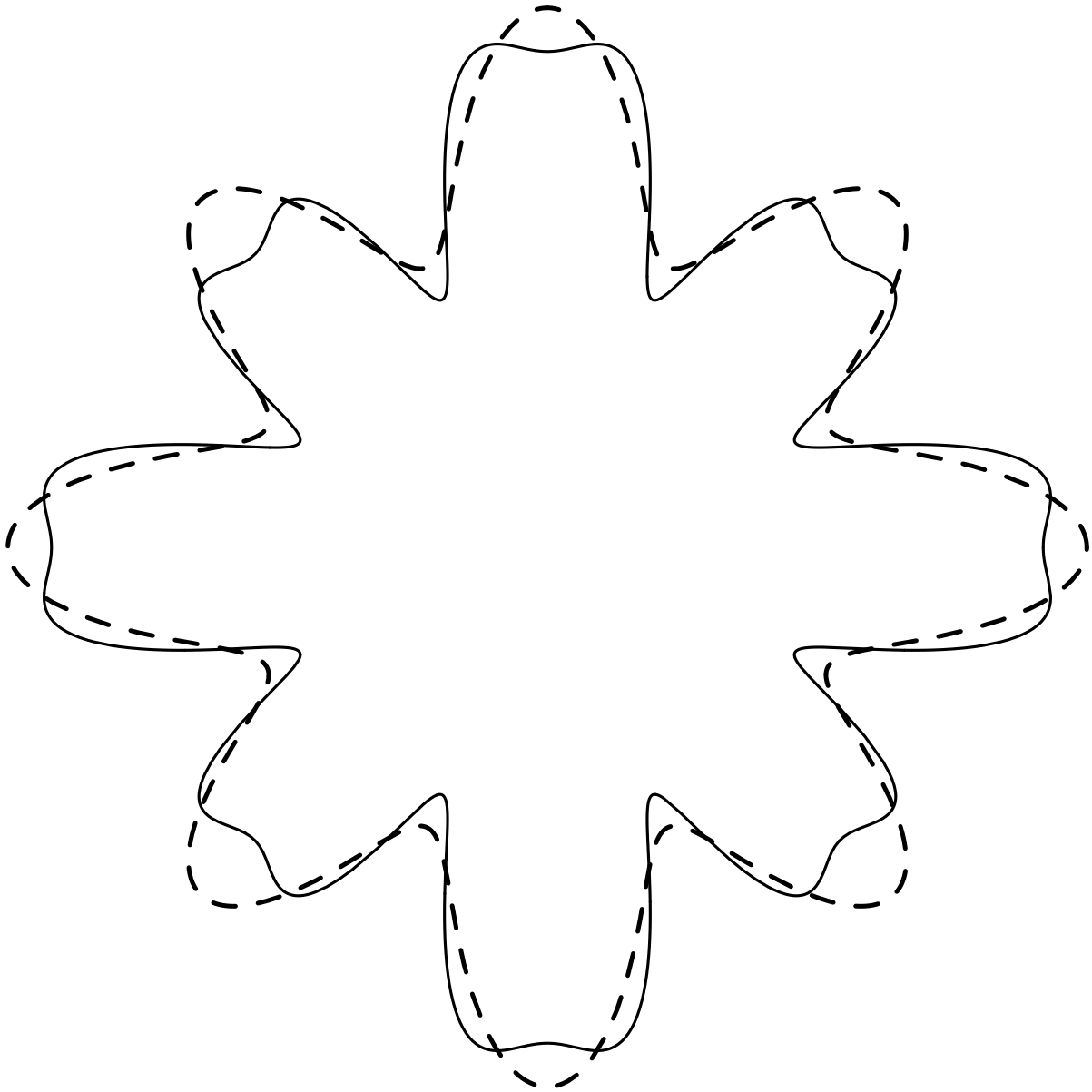


FIGURE 4

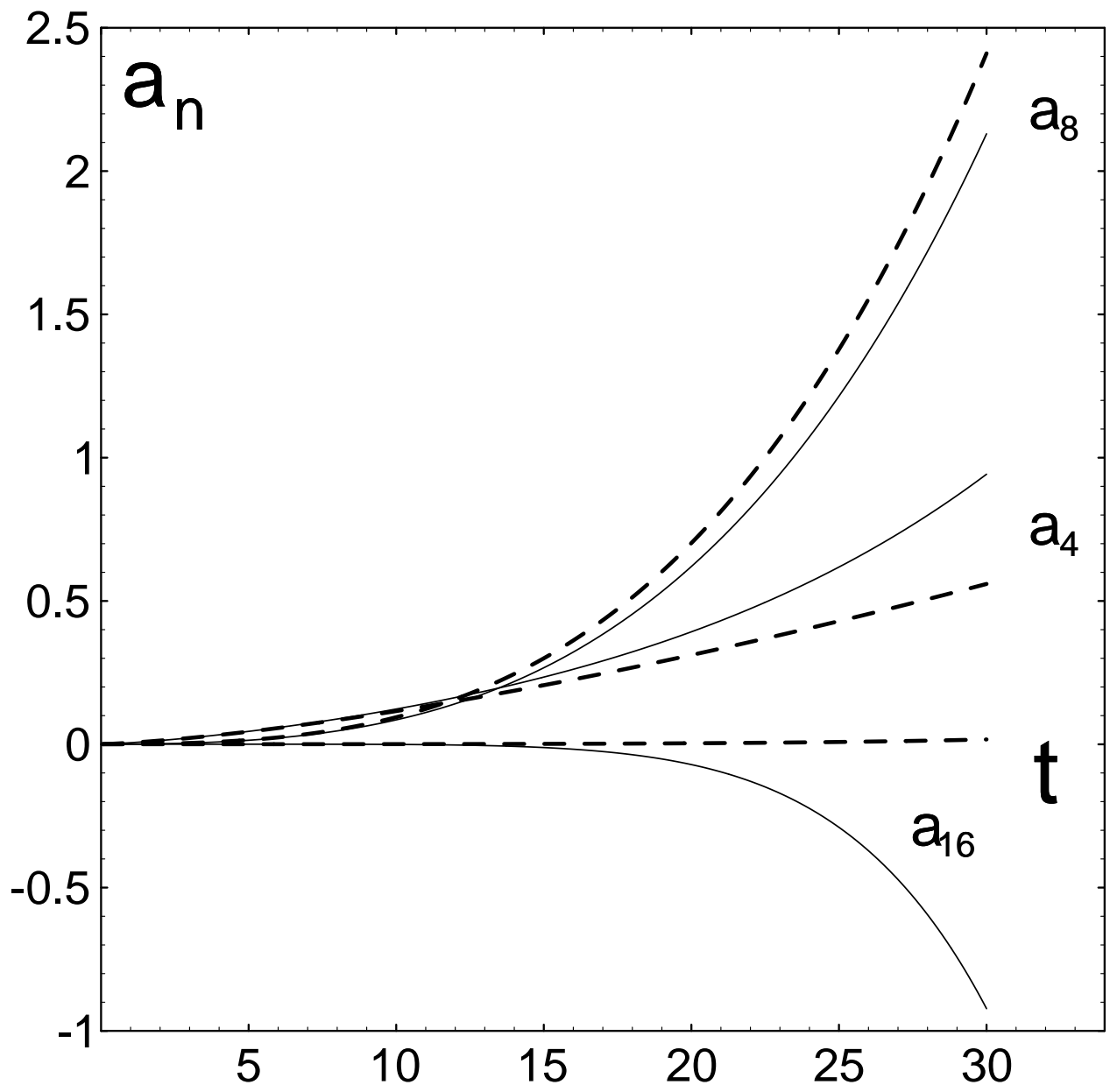


FIGURE 5